J. Fluid Mech. (1999), *vol.* 401, *pp.* 293–310. Printed in the United Kingdom

Coalescence of liquid drops

By JENS EGGERS[1], JOHN R. LISTER[2] AND HOWARD A. STONE[3]

[1] Universität Gesamthochschule Essen, Fachbereich Physik, 45117 Essen, Germany

[2] Department of Applied Mathematics and Theoretical Physics, University of Cambridge, Silver St, Cambridge CB3 9EW, UK

[3] Division of Engineering and Applied Sciences, Harvard University, Cambridge, MA 02138, USA

(Received 16 March 1999 and in revised form 28 July 1999)

When two drops of radius R touch, surface tension drives an initially singular motion which joins them into a bigger drop with smaller surface area. This motion is always viscously dominated at early times. We focus on the early-time behaviour of the radius r_m of the small bridge between the two drops. The flow is driven by a highly curved meniscus of length $2\pi r_m$ and width $\Delta \ll r_m$ around the bridge, from which we conclude that the leading-order problem is asymptotically equivalent to its two-dimensional counterpart. For the case of inviscid surroundings, an exact two-dimensional solution (Hopper 1990) shows that $\Delta \propto r_m^3$ and $r_m \sim (t\gamma/\pi\eta)\ln[t\gamma/(\eta R)]$; and thus the same is true in three dimensions. We also study the case of coalescence with an external viscous fluid analytically and, for the case of equal viscosities, in detail numerically. A significantly different structure is found in which the outer-fluid forms a toroidal bubble of radius $\Delta \propto r_m^{3/2}$ at the meniscus and $r_m \sim (t\gamma/4\pi\eta)\ln[t\gamma/(\eta R)]$. This basic difference is due to the presence of the outer-fluid viscosity, however small. With lengths scaled by R a full description of the asymptotic flow for $r_m(t) \ll 1$ involves matching of lengthscales of order r_m^2, $r_m^{3/2}$, r_m, 1 and probably $r_m^{7/4}$.

1. Introduction

There has been considerable interest recently in the breakup of free-surface flows into drops under the action of surface tension (Rallison 1984; Stone 1994; Eggers 1997). Here we investigate the complementary problem of surface-tension-driven coalescence of two drops, which is of fundamental importance in understanding the possible topological transitions in three-dimensional free-surface flows. For example, numerical implementations of merging (LaFaurie *et al.* 1994) are based on phenomenological prescriptions for joining the two surfaces, without a fundamental understanding or description of the dynamics.

Traditional applications of coalescence ideas include the description of two-phase dispersions. As an important example, we mention phase separation in two-phase flows (Nikolayev, Beysens & Guenoun 1996; Bonnecaze, Martula & Lloyd 1998), where the velocity field induced by the merging of two drops entrains other drops, thus enhancing the rate of coalescence. Another classical problem connected with drop coalescence is sintering, i.e. the merging of a powder into a homogeneous material by heating. In many cases, in particular that of ceramics or glasses, bulk fluid motion is the dominant mechanism for coalescence and the dynamical process is known

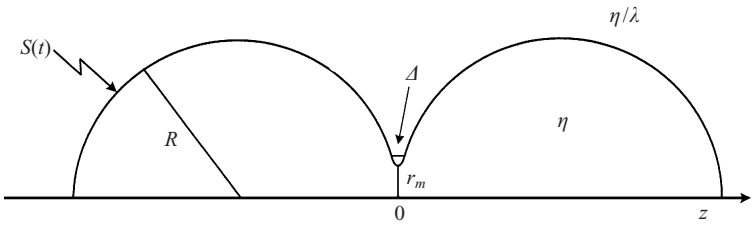

FIGURE 1. The surface profile produced by two coalescing drops of radius R. The origin of the axis of symmetry $z = 0$ lies at the initial point of contact. The bridge joining the two spheres has radius r_m and width Δ.

as viscous sintering. In a classical paper, Frenkel (1945) posed the problem of the merging of two spheres by slow fluid motion as the first step towards understanding the properties of the material that results from sintering. For a different case in which surface diffusion is the dominant mechanism of mass transport, the asymptotics of coalescence has recently been worked out (Eggers 1998), but such surface-dominated transport is very different from the bulk fluid motion of interest here.

Much of the experimental and numerical work on coalescence in viscous systems is motivated by the viscous sintering problem. An exception is an experimental paper (Bradley & Stow 1978) on the coalescence of water drops, but the low viscosity of water makes the motion very rapid and difficult to observe. On the other hand, by using a very high-viscosity fluid, the motion can be slowed down as much as desired (Brinker & Scherer 1990) and the experimental results agree very well with numerical simulations of the Stokes equations (Martinez-Herrera & Derby 1995). The only theoretical analysis of three-dimensional coalescence is the qualitative work by Frenkel (1945). Analytical solutions for two-dimensional coalescence (i.e. of parallel cylinders) have been obtained using complex variable techniques for the special case where the outer fluid is perfectly inviscid or absent (Hopper 1990, 1992, 1993*a*, *b*; Richardson 1992). We show below that the three-dimensional problem has the same asymptotic behaviour as this two-dimensional solution at early times. Our main aim, however, is to address the more general case of coalescence with a viscous outer fluid, for which we find that the structure of the solution near coalescence is quite different from the case of an inviscid exterior, though there is again a parallel between the two-dimensional and three-dimensional problems.

Part of the challenge in treating three-dimensional coalescence arises from the fact that it starts from a singular initial condition, shown in figure 1. We assume that the drops are initially spherical, which is based on an underlying assumption of negligible velocity of approach and hence negligible hydrodynamic deformation before contact. We imagine that two such drops have just been joined along their symmetry axis by some microscopic mechanism to form a tiny bridge of radius r_m. Evidently, the 'meniscus' around the bridge will be a region of very high curvature, which drives the increase of r_m with time. Our main concerns will be the time dependence of r_m for very early times, the shape of the interface, and the flow field near the meniscus. We note that the ratio of the coefficient of surface tension γ and the viscosity η gives a fixed velocity scale γ/η, and thus the expected Reynolds number $Re = \rho\gamma r_m/\eta^2$ will be be arbitrarily small as $r_m \to 0$, and the flow will initially be described by the Stokes equations regardless of the material parameters.

In the next section, we set up an integral representation of the Stokes flow and split it into two parts: an outer region far from the meniscus, in which the shape is still

close to the initial spherical condition, and an inner region near the meniscus in which the shape evolves rapidly. The dominant contribution to the velocity field comes from the high curvature of the meniscus, and its amplitude is determined by the lengthscale Δ of this curvature. The main task is thus to find the structure and scale of this inner solution. Since the inner solution is determined by the local curvature and not the global shape, the results obtained here are not restricted to the simple spherical geometry shown in figure 1. In § 3 we show that only a fraction of the fluid caught in the narrow gap between the two spheres is able to escape. The rest accumulates in a toroidal pocket, or 'bubble', of radius $r_b \propto r_m^{3/2}$ that forms at the meniscus. This bubble is connected to a thin 'neck' of width $r_n \propto r_m^2$. We have performed extensive simulations for the simplest case of equal-viscosity fluids which confirm these scaling laws.

In § 4 we examine the inner 'bubble' solution in greater detail. The bubble is joined to the neck by a short region of very large curvature on a lengthscale that appears numerically to be proportional to $(r_b r_n)^{1/2}$ and thus tends to a corner as $r_n/r_b \to 0$ (i.e. $r_m \to 0$). Though the curvature of this corner is much greater than that of the bubble, both contribute at the same order to the leading-order motion of the meniscus, which can be thought of as simply due to a ring force of strength 2γ smeared over a lengthscale r_b. In the final section we discuss the case of arbitrary viscosity ratios and mention related problems, namely, the effect of arbitrary initial shapes and the scaling at zero outer viscosity.

2. From three to two dimensions

For simplicity we consider two initially spherical drops of equal radii R, as shown in figure 1. Simple extensions to the cases of unequal radii and non-spherical shapes will be described in § 5. We denote the viscosity of the drops by η and that of the outer fluid by $\lambda^{-1}\eta$. As we have noted, the dynamics immediately after coalescence is described by the Stokes equations. Since these equations are linear, the velocity field can be expressed as an integral of the driving surface forces $\gamma\kappa\boldsymbol{n}$, where $\boldsymbol{n}$ is the normal directed into the outer fluid and $\kappa = \boldsymbol{\nabla}\cdot\boldsymbol{n}$ is the curvature of the interface. We make the velocity dimensionless with respect to γ/η, all lengths with respect to R, and times with respect to the corresponding timescale $\tau = R\eta/\gamma$.

Calculation of the evolution of the interface $S(t)$ requires only the interfacial velocity, which is given by the integral equation (Rallison & Acrivos 1978)

$$\frac{(1+\lambda^{-1})}{2}\boldsymbol{u}(\boldsymbol{x}_1) = -\int_{S(t)} \kappa \boldsymbol{J}\cdot\boldsymbol{n}\,\mathrm{d}\sigma_2 + (1-\lambda^{-1})\int_{S(t)} \boldsymbol{u}\cdot\boldsymbol{K}\cdot\boldsymbol{n}\,\mathrm{d}\sigma_2, \tag{1}$$

where

$$\boldsymbol{J}(\boldsymbol{r}) = \frac{1}{8\pi}\left[\frac{\boldsymbol{I}}{r} + \frac{\boldsymbol{rr}}{r^3}\right], \qquad \boldsymbol{K}(\boldsymbol{r}) = -\frac{3}{4\pi}\frac{\boldsymbol{rrr}}{r^5}, \quad \boldsymbol{r} = \boldsymbol{x}_1 - \boldsymbol{x}_2, \tag{2}$$

$\mathrm{d}\sigma_2$ denotes a surface area element at position $\boldsymbol{x}_2$, and $\boldsymbol{x}_1, \boldsymbol{x}_2$ both lie on $S(t)$. The first term on the right-hand side of (1) represents the driving by the surface forces, while the second accounts for the difference in viscosity between the fluids. The problem is closed by requiring that any material marker ξ with position $\boldsymbol{x}_1$ on the surface moves according to

$$\partial_t \boldsymbol{x}_1(\xi) = \boldsymbol{u}(\boldsymbol{x}_1). \tag{3}$$

Equation (1) and the identity

$$\int_S \boldsymbol{J}\cdot\boldsymbol{n}\,\mathrm{d}\sigma = \boldsymbol{0} \tag{4}$$

(which is a consequence of the incompressibility condition $\nabla\cdot\boldsymbol{J}=\boldsymbol{0}$) show that there would be no flow if κ were constant over S. It follows that, in the early stages of coalescence when $r_m \ll 1$, the flow is driven by the small region around the meniscus where κ is not close to its initial constant value of 2. This key observation motivates an analysis based on splitting the interface into two regions.

We use cylindrical polar coordinates (r,z) with origin at the junction between the drops. Away from the region of coalescence, the surface is essentially undisturbed and thus has the form $h(z)=(2z)^{1/2}$ and $h(z)=(-2z)^{1/2}$ for $r_m \ll h \ll 1$ in $z>0$ and $z<0$, respectively. The width of the gap between the spheres is given by

$$w = r^2 \qquad (r_m \ll r \ll 1), \tag{5}$$

and, since $\partial w/\partial r \ll 1$, the interfaces on either side of the gap are nearly parallel.

The solution for this outer region has to be matched with an inner solution on the scale $r = r_m$ of the bridge or meniscus where the two drops are joined. The inner solution has a region of very high curvature, which provides the dominant contribution to the velocity. To a first approximation, this region can be represented as a ring of radius r_m and small width Δ connected to two asymptotically straight interfaces each pulling outward with unit tension. The resultant effect is that of a radially directed ring force with strength 2 per unit length of the ring applied over a width Δ.

To find the velocity field generated by this ring, we try integrating over a circular line $\mathscr{L}$ of forces $\boldsymbol{f}(\boldsymbol{r}) = 2\boldsymbol{e}_r$. Considering, for the moment, only the simple case $\lambda = 1$, for which $\boldsymbol{u}$ can be computed directly from (1), we have

$$\boldsymbol{u}(\boldsymbol{x}_1) = \frac{1}{8\pi}\int_{\mathscr{L}} \left[\frac{\boldsymbol{f}(\boldsymbol{x}_2)}{|\boldsymbol{x}_1-\boldsymbol{x}_2|} + \frac{(\boldsymbol{x}_1-\boldsymbol{x}_2)(\boldsymbol{f}(\boldsymbol{x}_2)\cdot(\boldsymbol{x}_1-\boldsymbol{x}_2))}{|\boldsymbol{x}_1-\boldsymbol{x}_2|^3}\right]\mathrm{d}\sigma_2. \tag{6}$$

From this representation it is evident that the force distribution cannot be represented by a line everywhere as the first term in the integral (6) would lead to a logarithmically infinite value of the velocity. In the neighbourhood of r_m, when $|\boldsymbol{x}_2-\boldsymbol{x}_1| = O(\Delta)$, one must account for the fact that the force is distributed over a lengthscale of size Δ. The logarithmically dominant part of the integral, which comes from $\Delta \ll |\boldsymbol{x}_2-\boldsymbol{x}_1| \ll r_m$, gives a radially directed flow

$$\boldsymbol{u}(r_m) = -\frac{1}{2\pi}\ln\left(\frac{\Delta}{r_m}\right)\boldsymbol{e}_r. \tag{7}$$

Since the curvature of the ring is not apparent at leading order in the region $\Delta \ll |\boldsymbol{x}_2-\boldsymbol{x}_1| \ll r_m$ that dominates (7), we may equivalently consider the corresponding two-dimensional problem, in which coordinates (x,y) take the place of (z,r). In that case (two parallel cylindrical drops connected along a narrow band of width $2r_m$) the high-curvature meniscus is represented by two straight lines a distance $2r_m$ apart. Since the forces 2γ on the lines pull in opposite directions, they cancel on scales much greater than their distance apart, the integral (6) is cut off on the scale r_m, and (7) again results. Because of this asymptotic equivalence of the two-dimensional and axisymmetric problems, we will mostly consider the two-dimensional problem from now on, which is simpler numerically. The two-dimensional forms of the kernels $\boldsymbol{J}$

and $\boldsymbol{K}$ can be derived by integrating (2) along the third dimension to obtain

$$\boldsymbol{J}(r) = \frac{1}{4\pi}\left[-\boldsymbol{I}\ln r + \frac{\boldsymbol{rr}}{r^2}\right], \qquad \boldsymbol{K}(\boldsymbol{r}) = -\frac{1}{\pi}\frac{\boldsymbol{rrr}}{r^4}, \qquad \boldsymbol{r} = \boldsymbol{x}_1 - \boldsymbol{x}_2, \tag{8}$$

and the surface integral (1) is now along the perimeter of the two-dimensional drops.

Not only does (7) give the leading-order velocity in both two and three dimensions, but it should also hold for all viscosity ratios λ provided that the drops have non-zero viscosity ($\lambda \neq 0$). The argument, summarized below, has two components. First, it is clear that the early flow can always be thought of as driven by ring or line forces of strength $2\boldsymbol{e}_r$ or $2\boldsymbol{e}_y$ acting on some lengthscale Δ. Since Stokes flow has no inertia ($\nabla\cdot\boldsymbol{\sigma} = \boldsymbol{0}$), this force is transmitted unaltered across any surface enclosing the bubble and, since the width of the gap between the spheres is asymptotically negligible, the force must be supported almost entirely by the internal fluid of the spheres, and not by the external fluid in the narrow gap. (The special case $\lambda = 0$ is discussed in § 5.) Thus on the range of scales $\Delta \ll r - r_m \ll r_m$, the flow is the same at leading order as that of a ring or line force in a uniform fluid with the internal viscosity. Second, since it is this range that contributes the logarithmically dominant contribution to the velocity of a ring or line force, the coefficient of the logarithm in the leading-order flow is $\frac{1}{2}\pi$ independent of λ. The external viscosity does, of course, play a role in determining the subdominant $O(1)$ contribution from scales $r - r_m = O(\Delta)$. If the lack of dependence on λ of the dominant logarithmic part seems surprising, it may be noted that the same lack of dependence can be seen explicitly in the solution for the motion of a cylinder of one fluid through another fluid (Lister & Kerr 1989), where λ again affects only the $O(1)$ corrections. We conclude that (7) is correct at leading order for arbitrary λ and not just $\lambda = 1$.

To evaluate the velocity from (7), however, it is necessary to determine the scale Δ over which the force is distributed at the meniscus and here the viscosity ratio does play a role. In the following section we will show that $\Delta \propto r_m^{\alpha}$, where $\alpha = \frac{3}{2}$ for finite λ and $\alpha = 3$ for the special case $\lambda = \infty$ (no outer fluid). By integrating (7), we find that

$$r_m(t) \sim -\frac{(\alpha - 1)}{2\pi} t \ln t. \tag{9}$$

Recalling that time is measured in units of $\eta R/\gamma$, we see that the estimate based on dimensional analysis alone, $r_m \propto t\gamma/\eta$ is not quite correct, and in fact requires a logarithmic correction (which in dimensional terms brings in the drop radius R). Equation (9) is an asymptotic statement for $t \to 0$, whose validity rests on two assumptions. First, the scale Δ must be much smaller than r_m, so that the forcing almost exclusively comes from the meniscus. Second, the scaling assumption $\Delta \propto r_m^{\alpha}$ must hold. For $\lambda = 1$ and $\lambda = \infty$ the complete solution shows that (9) is a reasonable approximation for $r_m \lesssim 0.03$. In the case of a very small but finite outer viscosity, however, the predicted scaling $\alpha = \frac{3}{2}$ is observed only for $r_m \lesssim \lambda^{-2/3}$, as explained in § 5. Separate considerations also apply to the case of a very small inner viscosity.

3. Asymptotic shape of the meniscus

Using the equivalence of the two- and three-dimensional problems, we now study the coalescence of two viscous circular cylinders in more detail. Figure 2 compares Hopper's exact solution for $\lambda = \infty$ with a numerical simulation for $\lambda = 1$ in which the initial condition is that of a cusp with $r_m = 10^{-3}$, smoothed on the scale of r_m^2. (The numerical method is described in more detail below.) The shape of the meniscus for

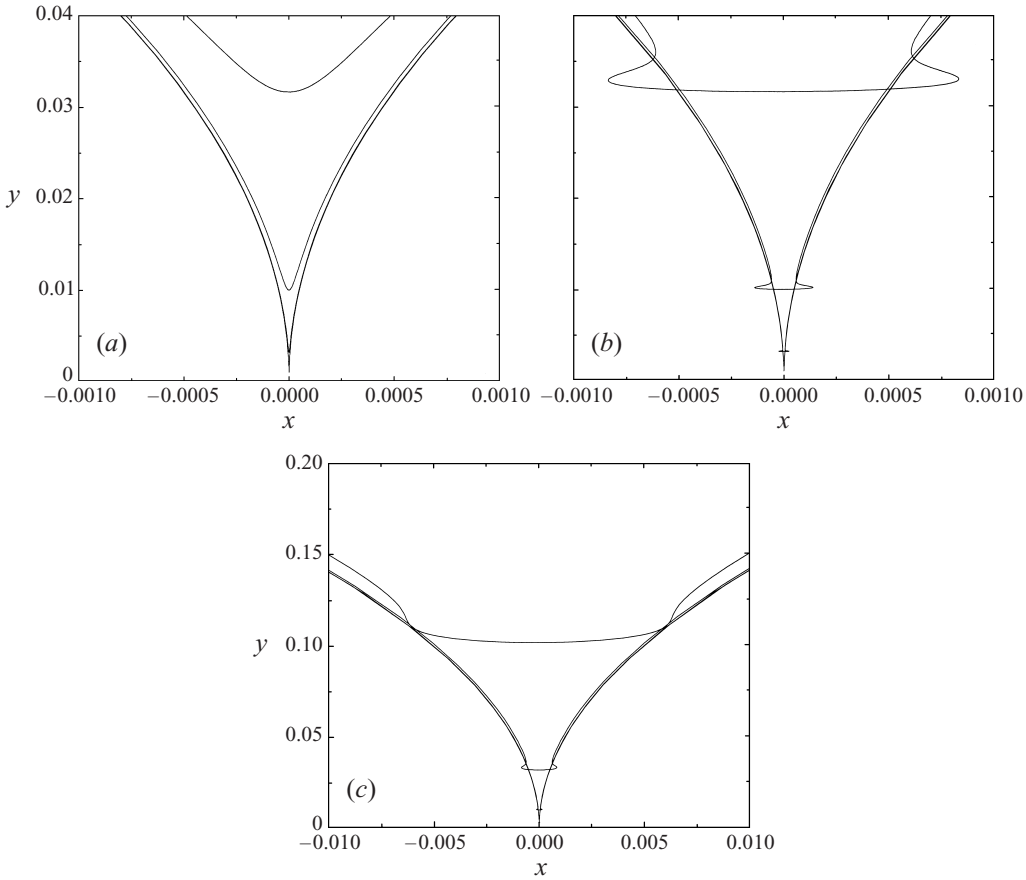

FIGURE 2. A closeup of the point of contact during coalescence of two identical cylinders for the two cases of no outer fluid ($\lambda = \infty$) and two fluids of equal viscosity ($\lambda = 1$). (*a*) Hopper's solution for $r_m = 10^{-3}, 10^{-2.5}, 10^{-2}$, and $10^{-1.5}$. (*b*) A numerical simulation of the viscosity-matched case that shows fluid collecting in a bubble at the meniscus. Note that the two axes are scaled differently, so the bubble is more circular than it appears. For $r_m \geqslant 0.1$, as shown in (*c*), the fluid finally escapes from the bubble, and the width of the meniscus is closer to the value of the gap width $O(r_m^2)$.

$\lambda = \infty$ is the tip of a near cusp (figure 2*a*), while the shape for $\lambda = 1$ is observed to be quite different for most of the evolution (figure 2*b*): the external fluid is collected in a small bubble at the meniscus, making the lengthscale Δ of the local solution much larger than in the absence of an external fluid. Only for $r_m > 0.1$ does the fluid caught inside the bubble escape and the profile becomes single-valued as the gap width widens (figure 2*c*).

3.1. *Analysis for an inviscid exterior*

The existence of an exact two-dimensional solution for the special case $\lambda = \infty$ of an inviscid or absent external fluid (Hopper 1993*a*, *b*; Richardson 1992) allows us to test the general ideas of § 2. Asymptotic expansion of this solution near the meniscus shows that

$$h(x) \sim \left[\tfrac{1}{2}r_m^2 + \sqrt{\left(\tfrac{1}{2}r_m^2\right)^2 + (2x)^2}\right]^{1/2} \qquad (x \ll 1), \tag{10}$$

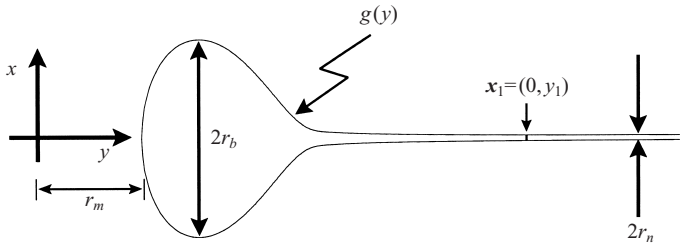

FIGURE 3. The structure of the local solution close to the meniscus. It resembles a bubble connected to a thin neck. The radius of the bubble is r_b and the minimum radius of the neck is r_n. The distance from the origin to the front of the bubble is r_m, which is not drawn to scale here.

from which we deduce that the highly curved region is of size $\Delta \sim r_m^3$, and the curvature κ scales like $\Delta^{-1} \sim r_m^{-3}$. This result is somewhat surprising since Δ is much smaller than the gap width $w \sim r_m^2$ estimated from the spherical shape of the outer solution and, at present, we do not have an asymptotic argument for the appearance of the small scale r_m^3. (By contrast, with a viscous outer fluid $\Delta \sim r_m^{3/2}$ is *larger* than the gap width w, and this scale can be understood from mass conservation as discussed in § 3.2.)

Inserting $\Delta \sim r_m^3$ into (7), we obtain

$$v_m \sim -\frac{1}{\pi} \ln r_m \tag{11}$$

for the velocity ($v_m = \dot{r}_m$) at the meniscus, which agrees with the asymptotic result given by Hopper (1993*a*); our earlier asymptotic analysis now allows the extension of this result to three dimensions.

3.2. *Analysis for a viscous exterior*

For the case $\lambda = 1$ we begin by discussing the structure of the local solution close to the meniscus, which is shown in figure 3. It consists of a 'bubble' of outer fluid of radius $\Delta \equiv r_b$, which is connected to a thin neck of width r_n. The neck matches onto the static outer solution, so r_n must scale like the gap width $w \sim r_m^2$. The area of the original gap up to r_m is $O(r_m^3)$ so that, if the meniscus advances faster than fluid can escape from the gap, the bubble should contain a finite fraction of the gap fluid and hence $r_b \sim r_m^{3/2}$.

To examine this argument in more detail, we consider the velocity field generated by the large curvature of the meniscus. As we have already noted, the flow is driven by that part of the interface where the interfacial curvature is significantly different from 1 (or 2 in the spherical case), namely $|r - r_m| = O(r_b)$. Using a multipole expansion of this forcing, we find the velocity field $\boldsymbol{u}(\boldsymbol{x}_1)$ at a distance $|\boldsymbol{x}_1 - \boldsymbol{x}_m| \gg r_b$ from the centre $\boldsymbol{x}_m$ of the bubble to be

$$\boldsymbol{u}(\boldsymbol{x}_1) = \boldsymbol{f} \cdot \boldsymbol{J}(\boldsymbol{x}_1 - \boldsymbol{x}_m), \tag{12}$$

at leading order, where $\boldsymbol{J}(\boldsymbol{r})$ is given by (8) and $\boldsymbol{f}$ is the total force exerted by the bubble. This force is the integral of $-\kappa \boldsymbol{n} = \partial_s \boldsymbol{t}$ over the bubbles' surface ($\mathscr{L}_b$), where $\boldsymbol{t}$ is the tangent vector pointing in the direction of increasing arclength s:

$$\boldsymbol{f} = -\int_{\mathscr{L}_b} \kappa \boldsymbol{n} \, \mathrm{d}\sigma = \int_{\mathscr{L}_b} \partial_s \boldsymbol{t} \, \mathrm{d}\sigma = \boldsymbol{t}_2 - \boldsymbol{t}_1. \tag{13}$$

In the present case $-\boldsymbol{t}_1 = \boldsymbol{t}_2 = \boldsymbol{e}_y$, so that the far-field velocity resulting from the

forcing of the bubble and its image is

$$\boldsymbol{u}(\boldsymbol{x}_1) = 2[\boldsymbol{J}(\boldsymbol{x}_1 - \boldsymbol{x}_m) - \boldsymbol{J}(\boldsymbol{x}_1 + \boldsymbol{x}_m)] \cdot \boldsymbol{e}_y. \tag{14}$$

We are interested in the flow in the neck, so we choose $\boldsymbol{x}_1 = (0, y_1)$ with $y_1 - r_m \gg r_b$. From (8) and (14) we find that the y-component of velocity in the neck is given by

$$u_n(y_1) = -\frac{1}{2\pi} \ln\left(\frac{y_1 - r_m}{y_1 + r_m}\right). \tag{15}$$

The representation (15) breaks down when $y_1 - r_m = O(r_b)$, since the higher-order terms in the multipole expansion become of comparable magnitude and $u_n(y_1)$ crosses over to some function that depends on the detailed structure of the bubble. Since (15) must match onto the velocity field in the bubble, we can write the velocity of the meniscus as

$$v_m = v_0 + \frac{1}{2\pi} \ln\left(\frac{2r_m}{r_b}\right), \tag{16}$$

where the constant v_0 comes from the detailed shape of the bubble, and for $\lambda = 1$ is found numerically to be $v_0 = -0.077$. (This equation is consistent with (7), but also includes a representation of the $O(1)$ contribution.)

If $r_b \ll y_1 - r_m \ll r_m$ then from (15) and (16)

$$u_n(y_1) \approx \frac{1}{2\pi} \ln\left(\frac{2r_m}{y_1 - r_m}\right) \ll \frac{1}{2\pi} \ln\left(\frac{2r_m}{r_b}\right) \approx v. \tag{17}$$

Thus the fluid in the neck ahead of the bubble only starts to move at a speed comparable to that of the bubble when $y_1 - r_m = O(r_b)$, i.e. when the bubble has caught up with it. Thus all the fluid in the neck is collected into the advancing and growing bubble. Since the neck width r_n scales like r_m^2, the total area of neck collected scales like r_m^3, and thus

$$r_b \sim r_m^{3/2}. \tag{18}$$

Finally, combining (18) with (16) or (9), we find that

$$v_m \sim -\frac{1}{4\pi} \ln r_m, \tag{19}$$

which can be integrated to give

$$r_m \sim -\frac{t}{4\pi} \ln t. \tag{20}$$

This result differs by a factor of 4 from the $\lambda = \infty$ limit.

3.3. *Numerical tests of scaling*

To test the predictions of these scaling ideas, we have performed extensive two-dimensional simulations of drop coalescence using the boundary-integral method. The initial bridge has $r_m(0) = 10^{-6}$, which means the gap width is $w = 10^{-12}$ initially. For simplicity, we only considered the viscosity-matched case $\lambda = 1$ so that the second term drops out from (1) and $\boldsymbol{u}$ can be computed directly from the surface forces without having to solve a matrix equation. The interface was parameterized by arclength, and derivatives were evaluated using centred differences. The interface was advanced according to (3), using an explicit second-order Runge–Kutta step. The difference between the result of time step Δt and two half-steps $\Delta t/2$ was used to control the time step.

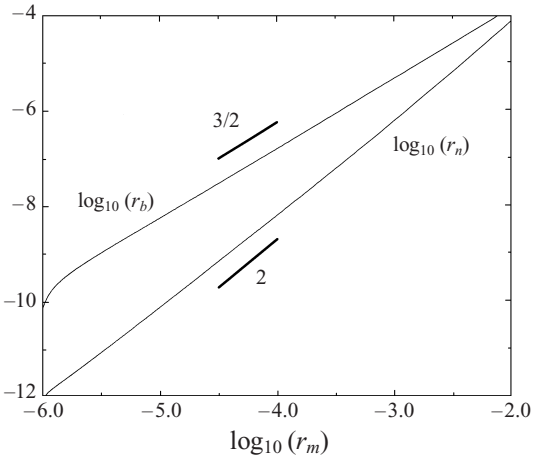

FIGURE 4. Scaling of the bubble radius r_b and the neck radius r_n as function of r_m.

Improvement of the stability of our numerical method by making it implicit would be computationally very demanding for an integral operator. Instead, we use a scheme first proposed by Douglas & Dupont (1971). The equation of motion (3) for the position of the interface can be written at any given time as a linearization around the current interfacial position $\boldsymbol{x}_0$:

$$\partial_t \boldsymbol{x} = \boldsymbol{A}(\boldsymbol{x}) \cdot (\boldsymbol{x} - \boldsymbol{x}_0) + \text{constant}. \tag{21}$$

By writing this as

$$\partial_t \delta\boldsymbol{x} = (\boldsymbol{A} - \boldsymbol{B})\delta\boldsymbol{x} + \boldsymbol{B}\delta\boldsymbol{x} + \text{constant} \tag{22}$$

and treating the first part explicitly, but the second part implicitly, the scheme becomes unconditionally stable as long as $|\boldsymbol{B}| > |\boldsymbol{A}|/2$, where the matrix norm is defined to be the modulus of the largest eigenvalue (Douglas & Dupont 1971). In the present case, $|\boldsymbol{A}|$ scales like $(\Delta x)^{-1}$ up to logarithmic corrections, where Δx is the minimum grid spacing. By choosing $\boldsymbol{B}$ to be a diffusion operator multiplied by the local grid spacing, one can make sure that the numerical method, although treating the integral operator explicitly, becomes unconditionally stable. Without the help of this trick the time steps required to integrate the equation of motion from $r_m = 10^{-6}$ to $r_m = 10^{-4.5}$ would have been prohibitively small.

To achieve the necessary spatial resolution, local refinement of the mesh is crucial. The resolution near the meniscus was set by the inverse of the local curvature. Away from the inner solution, the grid spacing was allowed to taper off geometrically, with the spacing constrained to change by no more than 10% from one grid point to the next. As explained in more detail below, additional resolution was used in the transition region where the bubble merges into the neck. The maximum number of points used to represent one quadrant of the shape was about 900. Every few time steps a new grid was constructed using the current interface, and the interface was interpolated to the new grid. Thus there was no need to rearrange the grid points along the interface.

In figure 4 we show the scaling of the bubble radius r_b and the minimum neck radius r_n and observe that both follow the predicted power laws (18). A closer inspection shows that the slope of $\log r_b$ is slightly smaller than expected, which is because the scaling of the area of the bubble is almost the same as that of the neck. (The portion

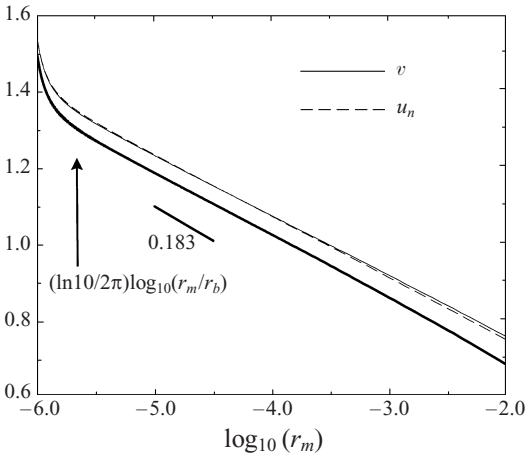

FIGURE 5. Scaling of the velocity v at the tip and the velocity u_n at a position $y = r_m + 20r_b$ in the neck. There is a constant difference of 0.4 between the two. Both agree very well with the scaling of $(1/2\pi)\ln(2r_m/r_b)$ as predicted by theory. For comparison, we also give a slope of $(\ln 10)/4\pi = 0.183$.

of the neck up to the point $y = r_m + ar_b$ contributes an area $A_n \approx ar_b r_m^2 \sim r_m^{7/2}$, which is only slightly smaller than $A_b \approx r_m^3$ since the two exponents are close.) We confirmed numerically that the r_m-dependence of the total area $A = A_b + A_n$ has no significant deviation from r_m^3, as expected.

The scaling of the velocity at the meniscus (v) and in the neck (u_n) at position $y_1 = r_m + ar_b$ is shown in figure 5 (with $a = 20$) and compared with $(1/2\pi)\ln(2r_m/r_b)$, which is predicted by equations (16) and (17) to have the same slope. The theory gives $v - u_n =$ constant $= \ln a/(2\pi) + v_0$ which is found numerically to be very close to 0.4 and hence $v_0 = -0.077$. All three curves in figure 5 should have a slope $(\ln 10)/4\pi$ when plotted against $\log_{10}(r_m)$. The noticeable deviation comes from the fact that one is effectively taking the *difference* between $\log_{10} r_m^{3/2}$ and $\log_{10} r_m$, so non-asymptotic effects in r_b, still present on these small scales, become more pronounced.

It has been implicit in the previous arguments that the inner solution, consisting of a bubble connected to a thin neck, has reached its asymptotic form: in the frame of reference of the advancing bubble tip, and rescaled by the bubble radius, the shape should be stationary. Figure 6, showing both the local interface profile and the curvature at two values of r_m a factor of ten apart, reveals that there is, in fact, a slow variation in part of the local profile. This slow variation is seen as a positive second peak in the curvature at the point where the bubble meets the neck. To be able to resolve scales down to $r_m = 10^{-6}$, additional grid points were inserted at the position of the second peak, where the grid spacing was based on the width of the peak. As $r_m \to 0$, which corresponds to going back in time, the second curvature peak increases and also gets narrower, as its integral must be finite to yield a finite change of slope.

To obtain more information about the asymptotic shape of the inner solution and the growth of the secondary peak in curvature, it is useful to consider the inner solution as a separate problem. This analysis is given in the next section.

4. Bubble on a neck

Here we study the local solution close to the meniscus, which consists of a bubble of radius r_b connected to a thin neck of width r_n (see figure 3). Asymptotically, the

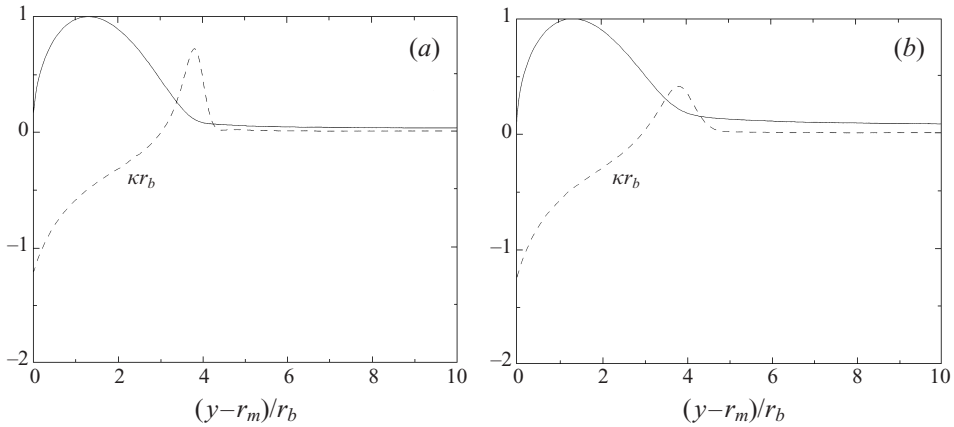

FIGURE 6. The local solution (solid) and its curvature distribution (dashed) in coordinates rescaled by r_b. As r_m gets smaller, a sharp peak develops at the junction between the bubble and the neck. (*a*) $r_m = 10^{-4.5}$, (*b*) $r_m = 10^{-3.5}$.

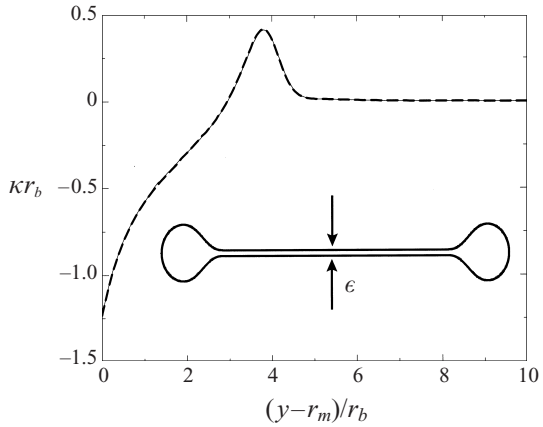

FIGURE 7. A comparison of the curvature distribution of the local solution for $r_m = 10^{-3.5}$ and the stationary 'bubble on a neck'. The peak height of the positive curvature has been used to match the two. In an inset, we show the initial condition used to compute the stationary shape of the translating bubble.

curvature of the neck is very small compared with r_b^{-1}, so the neck can effectively be considered as an infinitely long channel of uniform width. For simplicity in computations, we apply reflective boundary conditions at some large distance down the neck, to arrive at the geometry depicted in the inset of figure 7. For the problem under consideration here, only one half of the configuration matters. From now on, all lengths will be measured in units of r_b, so the radius of the bubble is normalized to unity, and the radius of the neck asymptotes to some small number $\epsilon \approx r_n/r_b$. The solution we are interested in, which corresponds to the asymptotic structure described in § 3, is such that the interfacial shape $g(y,t)$ is advected at a quasi-steady speed v_c without changing its shape

$$g(y,t) = G(y - v_c t). \tag{23}$$

The physical meaning of this statement in the original problem is that the local solution relaxes to a quasi-steady state on a timescale proportional to $r_b \propto r_m^{3/2}$, while

the meniscus moves on a timescale proportional to r_m, which is much longer. Thus the velocity v_c, which varies logarithmically with time in the full problem, can be regarded as constant in (23). The velocity field of the local steadily translating shape (23) must satisfy

$$(u_y - v_c)G' = u_x. \tag{24}$$

The boundary condition is that $g(y)$ approaches ϵ as $y \to \infty$. The components of the velocity field u_x and u_y follow from the integral equation (1) as usual. Instead of solving the system (1) and (24) directly, we found it most convenient to evolve two bubbles attached to a very long, straight neck of radius ϵ_{init} until a stationary shape is established, as shown in the inset to figure 7. The tension in the neck is responsible for pulling the bubble along. The neck shortens during the relaxation and the radius increases to a value ϵ, which then only changes very slowly by the time a stationary shape is reached.

Since the radius of the bubble r_b and the radius of the neck r_n are very different, one might think that the curvature distribution within the bubble is independent of the neck radius ϵ. However, the limit $\epsilon \to 0$ turns out to be singular as an increasingly pronounced peak of positive curvature appears at the junction between bubble and neck, as demonstrated in figure 6.

First, in figure 7 we compare the curvature distribution as given in figure 6 for $r_m = 10^{-3.5}$ with that of the stationary problem, equations (1) and (24), with $\epsilon = r_n/r_b$. We choose ϵ_{init} such that the neck has the appropriate width ϵ by the time a stationary shape is reached. The excellent agreement shows that the flow close to the meniscus is completely equivalent to the translating bubble, which is of course a much simpler problem. Hence the inner solution of the coalescence problem can be understood completely in terms of the translating bubble.

Figure 8(*a*) shows a sequence of bubble shapes for increasingly small values of ϵ. The overall shape of the bubble does not depend very much on ϵ, and it looks as if the shapes are almost the same for the two smallest values. However, there is an increasingly sharp 'corner' at the point where the neck meets the bubble. This result is most evident from a plot of the curvature for the same values of ϵ; see figure 8(*b*). While the curvature of the bubble is negative, the corner at the junction between the bubble and the neck corresponds to a growing peak of positive curvature. In figure 8(*b*) we also include a plot of the maximum of this peak as a function of ϵ. The data suggest $\kappa^{-1} \sim \epsilon^{1/2}$ though it is hard to make a definite statement. If this is so then the lengthscale of the corner is the geometric mean of the scales of the bubble and the neck, which would be $r_m^{7/4}$ in the coalescence problem. From (13) it is evident that the total force exerted by the peak is equal to the change in slope. As can be seen from figure 8(*a*), this change is constant to a good approximation so that, of the total force $2\boldsymbol{e}_y$ exerted by the bubble, roughly 15% is exerted by the corner and 85% by the rest of the bubble.

5. Discussion and outlook

As we have demonstrated, even the simplest case of viscosity-matched fluids represents a problem of enormous complexity, in which there are features on at least the lengthscales r_m^2, $r_m^{3/2}$, r_m and 1. Therefore, we confined ourselves to computing the leading-order asymptotics, which we note are only logarithmically dominant. In all likelihood, quantities like the bubble radius $r_b(t)$ contain additional logarithmic terms, whose calculation requires a better knowledge of the matched asymptotics of

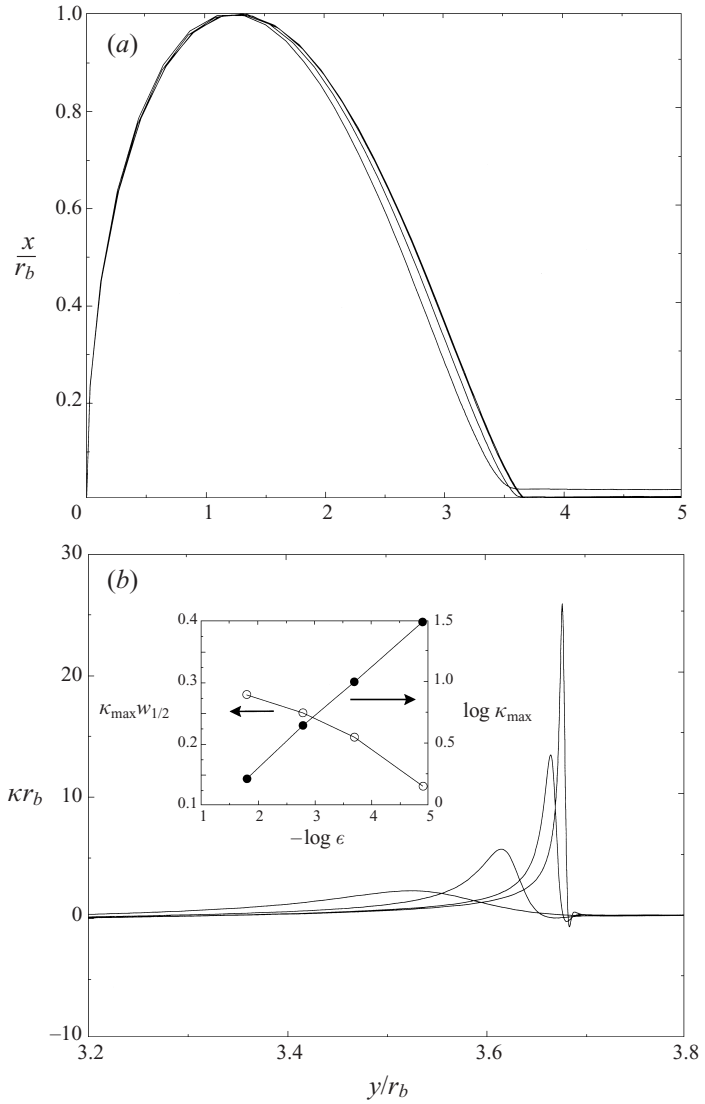

FIGURE 8. (*a*) The stationary state of a translating bubble, pulled by a thin neck for different values of $-\log_{10}\epsilon = 1.8, 2.8, 3.7$, and 4.9. (*b*) Blowup of the curvature distribution. Although the surface shape seems to have converged, the maximum negative curvature in the junction still increases. The insets show the scaling of the maximum curvature κ_{max} and that of $\kappa_{max} w_{1/2}$, where $w_{1/2}$ is the half-width measured in arclength.

the problem. Further complications arise because the inner solution is itself singular, with a corner of lengthscale which we estimate to be $O(r_m^{7/4})$. Important goals for future work would be confirmation of the inner scalings, formal asymptotic matching of the different scales, and to go beyond the leading-order problem.

Another important problem is the generalization of our calculations to arbitrary viscosity ratios λ. A major obstacle to developing a quantitative theory for general λ is that for $\lambda \neq 1$ equation (1) is a second-kind integral equation for the velocity field, which has to be solved at each time step. For small r_m a uniform translation of the coalescing drops in opposite directions is close to a solution of (1), apart from a

crossover in the neck region. This means that the matrix associated with solving (1) is very close to being singular. Even using a singular-value decomposition (Press *et al.* 1992), we have been unable to treat the singularity sufficiently well to go beyond r_m-values of 10^{-2} for $\lambda = 4$. Unfortunately, this is not sufficient to make definite statements about the scaling for small r_m.

We have argued already that we expect the leading-order behaviour of $\dot{r}_m$ to be given by (7) for any positive λ since the net force from the meniscus creates a logarithmically large velocity supported primarily by the internal fluid. We also believe that the scaling $\Delta \sim r_m^{3/2}$ will hold as $r_m \to 0$ for any finite λ since, even for large λ (small external viscosity), the pressure drop along a narrow channel is large and so the outer fluid is not able to escape from the gap and is caught in a bubble. Expressed differently, the positive curvature at the bubble corner is unable to pull the walls of the channel apart since this would require significant motion along the channel. It is intriguing that Hopper's exact solution shows that the situation is very different for $\lambda = \infty$ when there is no external viscous resistance to overcome and no bubble forms (figure 2*a*). Thus the limits $\lambda \to \infty$ and $r_m \to 0$ do not commute, reflecting the fact that one must be careful in assuming a zero-stress condition in situations involving narrow cusps, as even a very small external viscosity can be significant.

We can provide a physical estimate for the scale below which a bubble forms for $\lambda \gg 1$. Fluid motion in the narrow gap may be treated with the lubrication approximation, whence $\eta u_n/(\lambda r_n^2) \approx \Delta p/r_m$ and $\Delta p \approx \gamma/r_b$ gives the estimate $u_n \approx (\lambda\gamma/\eta)(r_m/R)^{3/2}$. Therefore, a bubble can only be expected to form when the meniscus motion $v \approx \gamma/\eta > u_n$, which occurs on an approximate lengthscale $r_m/R < \lambda^{-2/3}$. It is also interesting to consider the opposite limit $\lambda \to 0$, which corresponds to gas bubbles in a viscous fluid. For $\lambda = 0$, the viscous stresses generated by the inner fluid or gas are zero and the resistance to initial expansion of the contact meniscus is provided by radial compression of the viscous external fluid in the neck. It is not clear to us how this will affect the interfacial geometry. For any finite λ, on the other hand, there is a scale below which the sheet of viscous fluid in the neck is too thin to contribute significantly to the stress. Thus $\lambda \to 0$ also does not commute with $r_m \to 0$ and is a singular limit.

We have been considering the simplest case of equal spheres brought into contact. The case of unequal spheres of radii R and R/δ with $\delta < 1$ is a straightforward generalization in which the gap thickness (5) is simply replaced by

$$w = r^2(1+\delta)/2 \qquad (r_m \ll r \ll 1). \tag{25}$$

Just as in the case of equal spheres, for $r_m \ll 1$ the interfaces on either side of the gap are both nearly parallel to the y-axis. Thus all our asymptotic arguments remain the same, while the range of validity is set by the size of the smaller sphere, whose higher curvature comes into play first.

Similar considerations show that the early-time evolution of axisymmetric drops brought into contact along their symmetry axes depends only on the local curvature at the initial contact. A more interesting variation is that of general initial shapes for which the locus of high curvature (in three dimensions) near contact no longer forms a circle, but is a more general closed curve. To leading order, this curve is convected with a logarithmically large velocity field, pointing in the direction normal to the curve.

Recent research (Nikolayev *et al.* 1996; Bonnecaze *et al.* 1998) has suggested that the rate of coalescence in emulsions can be greatly enhanced by the flow generated by individual coalescence events. Our analysis suggests that an appropriate model

for the far-field velocity of a single coalescence event is the Stokes flow driven by an expanding ring force of radius r_m and strength 2γ per unit length, which makes sense for $\Delta \ll r_m$, and hence $r_m \lesssim 0.1$. This dipolar flow, which in the case $\lambda = 1$ may be obtained by solving

$$\eta \nabla^2 \boldsymbol{u} - \nabla p + 2\gamma \delta(r - r_m)\delta(z)\boldsymbol{e}_r = \boldsymbol{0} \tag{26}$$

using Hankel transforms (Stone & Brenner 1996), is

$$\left.\begin{aligned} u_r(r,z) &= \frac{\gamma r_m}{2\eta}\int_0^\infty J_1(kr)J_1(kr_m)(1-kz)\mathrm{e}^{-kz}\,\mathrm{d}k, \\ u_z(r,z) &= -\frac{\gamma r_m}{2\eta}\int_0^\infty J_0(kr)J_1(kr_m)kz\mathrm{e}^{-kz}\,\mathrm{d}k, \\ p(r,z) &= 2\eta u_z(r,z)/z, \end{aligned}\right\} \tag{27}$$

where the J_n are Bessel functions. These equations can be approximated in the limit $r_m \ll (r^2+z^2)^{1/2}$ to obtain the axisymmetric dipole

$$\boldsymbol{u}(r,z) \approx \frac{\gamma r_m^2}{4\eta}\frac{(r^2-2z^2)}{(r^2+z^2)^{5/2}}\left[r\boldsymbol{e}_r + z\boldsymbol{e}_z\right], \tag{28}$$

which is shown in figure 9 superimposed on the outlines of two spherical bubbles. If one is not interested in the full solution (27), (28) may also be obtained directly from (6) by expanding the kernel and integrating over the ring. The coalescence-induced radially directed force drives a flow towards the two drops over an angle $\approx 127^\circ$. The flow (28) might be used for simplicity in models of multiple coalescence.

All motions described so far begin with a local point contact and it is worth considering how this contact might be achieved. The near-contact squeezing motion generated when two drops (or a drop and a plane) are in relative motion can be analysed using the lubrication approximation or numerical simulations (e.g. Jones & Wilson 1978; Yiantsos & Davis 1991; Rother, Zinchenko & Davis 1997). Owing to the large pressures accompanying flow along the narrow gap, the surface tends to deform in the narrow gap. In particular, when two equal-size drops are squeezed together with a force F on each drop, then a dimple tends to form when $h_0(t) < R/\lambda^2$, where $h_0(t)$ is the minimum gap spacing and R the radius of curvature of the undeformed drop. The magnitude of the deformation becomes the same order of magnitude as the gap height and the dimple has a radial scale $\left(FR/\gamma\right)^{1/2}$. Away from the gap the drop is nearly spherical so long as, for $\lambda = O(1)$, the effective capillary number is small, $O(Fh_0^{1/2}/\gamma R^{3/2}) \ll 1$. An implication of these analyses is that contact is very likely to occur along a rim, or at least at an off-axis position, with an initial radius of the bridge of order $\left(FR/\gamma\right)^{1/2}$. The dynamics would then follow the results shown in § 3. A tiny droplet of the exterior fluid from the dimple is left behind near the centre of the coalescing drops.

From an experimental point of view, it is probably not relevant to investigate smaller (dimensionless) r_m than 10^{-5} since the gap width just ahead of the bubble is proportional to r_m^2, which is then of microscopic size for reasonable values of R. Very small inhomogeneities in the fluid or van der Waals attractions will cause the two interfaces to reconnect, and to create an instability that breaks the azimuthal symmetry we have assumed in the three-dimensional problem. Moreover, the bubble actually forms a structure that resembles a long thin torus in three dimensions, and is thus prone to a Rayleigh capillary instability, which grows on a short timescale proportional to r_b and is potentially dangerous. On the other hand, there are stabilizing

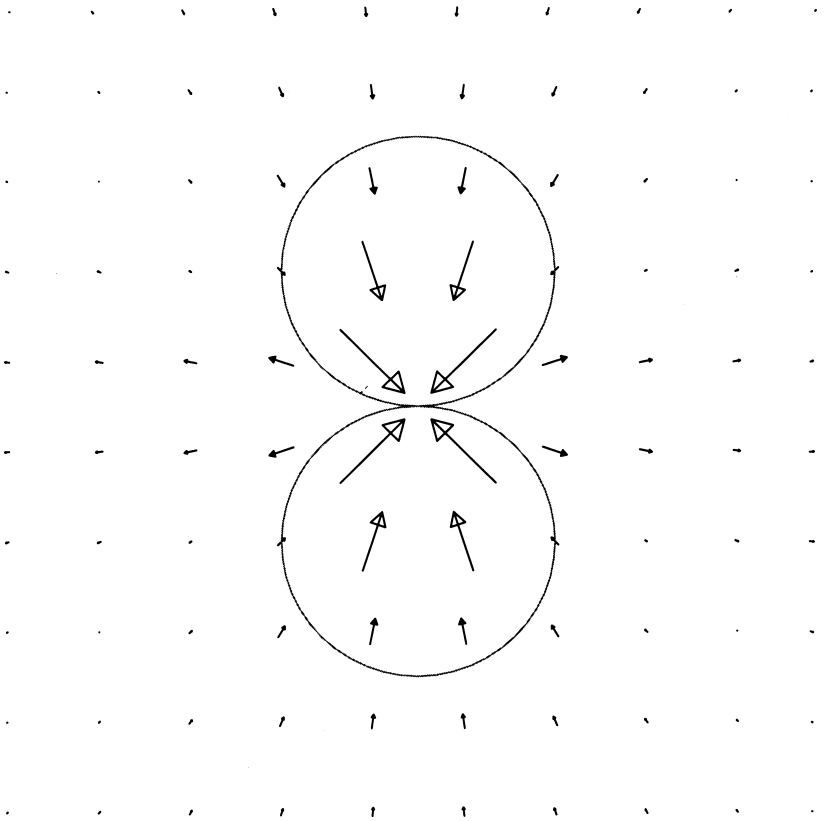

FIGURE 9. The velocity field generated by an expanding ring of forces in the limit of the radius of the ring r_m going to zero. Note that the velocity field is pointing outward in the direction of the expanding ring, but is inwardly directed over much of the flow domain.

effects since the bubble is also convected (Brenner, Shi & Nagel 1994), and a careful nonlinear stability analysis has to be done to determine the scale where the stability is first expected to occur. This question is experimentally relevant because it sets the size of small bubbles of the outer fluid that may be observed after coalescence.

We have pointed out that coalescence is initially described by the Stokes equations. If the viscosity of the fluid is small, this is true only for the early stages of coalescence, until the Reynolds number is of order one, which happens when

$$r_m \approx \ell, \quad \ell = \eta^2/(\rho\gamma). \tag{29}$$

For water, $\ell = 1.4 \times 10^{-6}$ cm , so it is a very relevant question to go beyond the Stokes approximation. After passing the transition region (29) we expect the dynamics to be described by the Euler equations. Assuming that the scale of the local solution at the meniscus is set by the gap width alone, the interfacial stress driving this motion is approximately $\gamma/(r_m^2/R)$, which is to be the same magnitude as ρv^2. Hence, with $v = \dot{r}_m$, we find

$$r_m \propto \left(\frac{\gamma R}{\rho}\right)^{1/4} t^{1/2}, \tag{30}$$

which corresponds to $v \propto t^{-1/2}$. The geometrical part of both problems is similar to the Stokes case, but the coupling between pressure and velocity makes the relationship

between the surface shape and the velocity different, so an alternative treatment is needed to predict the numerical coefficient in front of the power law for r_m.

Clearly, the possibility of finite Reynolds number, arbitrary surface shape, finite velocity of approach, and the inclusion of another fluid outside the drops lends a tremendous richness to the class of singularities studied here.

We are indebted to Stephane Zaleski for bringing the authors together and for sharing his deep insight. J. E. and J. R. L. were visitors to LMM at the University of Paris VI, and H. A. S. to PCT at ESPCI. Denis Gueyffier helped us crucially by producing the first simulation of coalescing drops. Todd Dupont gave very helpful advice on the numerical simulations.

REFERENCES

Bonnecaze, R. T., Martula, S. & Lloyd, D. R. 1998 Modeling of coalescence-induced coalescence. Presented at the 1998 AIChE Annual Meeting, Miami, Fl.

Bradley, S. G. & Stow, C. D. 1978 Collisions between liquid drops. *Phil. Trans. R. Soc. Lond.* A **287**, 635–675.

Brenner, M. P., Shi, X. D. & Nagel, S. R. 1994 Iterated instabilities during droplet fission. *Phys. Rev. Lett.* **73**, 3391–3394.

Brinker, C. J. & Scherer, G. W. 1990 *Sol-Gel Science*. Academic.

Douglas Jr., J. & Dupont, T. 1971 Alternating-direction Galerkin methods on rectangles. In *Numerical Solution of Partial Differential Equations – II* (ed. B. Hubbard), pp. 133–214. Academic Press.

Eggers, J. 1997 Nonlinear dynamics and breakup of free surface flows. *Rev. Mod. Phys.* **69**, 865–929.

Eggers, J. 1998 Coalescence of spheres by surface diffusion. *Phys. Rev. Lett.* **80**, 2634–2637.

Frenkel, J. 1945 Viscous flow of crystalline bodies under the action of surface tension. *J. Phys.* (*Moscow*) **9**, 385–391.

Hopper, R. W. 1990 Plane Stokes flow driven by capillarity on a free surface. *J. Fluid Mech.* **213**, 349–375.

Hopper, R. W. 1992 Stokes flow of a cylinder and half-space driven by capillarity. *J. Fluid Mech.* **243**, 171–181.

Hopper, R. W. 1993*a* Coalescence of two viscous cylinders by capillarity: Part I. Theory. *J. Am. Ceram. Soc.* **76**, 2947–2952.

Hopper, R. W. 1993*b* Coalescence of two viscous cylinders by capillarity: Part II. Shape evolution. *J. Am. Ceram. Soc.* **76**, 2953–2960.

Jones, A. F. & Wilson, S. D. R. 1978 The film drainage problem in droplet coalescence. *J. Fluid Mech.* **87**, 263–288.

Lafaurie, B., Nardone, C., Scardovelli, R., Zaleski, S. & Zanetti, G. 1994 Modelling merging and fragmentation in multiphase flows with SURFER. *J. Comput. Phys.* **113**, 134–147.

Lister, J. R. & Kerr, R. C. 1989 The effect of geometry on the gravitational instability of a buoyant region of viscous fluid. *J. Fluid Mech.* **202**, 577–594.

Martinez-Herrera, J. I. & Derby, J. J. 1995 Viscous sintering of spherical particles via finite element analysis. *J. Am. Ceram. Soc.* **78**, 645–649.

Nikolayev, V. S., Beysens, D. & Guenoun, P. 1996 New hydrodynamic mechanism for drop coarsening. *Phys. Rev. Lett.* **76**, 3144–3147.

Press, W. H., Teukolsky, S. A., Vetterling, W. T. & Flannery, B. P. 1992 *Numerical Recipes*. Cambridge University Press.

Rallison, J. M. 1984 The deformation of small viscous drops and bubbles in shear flows. *Ann. Rev. Fluid Mech.* **16**, 45–66.

Rallison, J. M. & Acrivos, A. 1978 A numerical study of the deformation and burst of a viscous drop in an extensional flow. *J. Fluid Mech.* **89**, 191–200.

Richardson, S. 1992 Two-dimensional slow viscous flows with time-dependent free boundaries driven by surface tension. *Eur. J. Appl. Maths* **3**, 193–207.

Rother, M. A., Zinchenko, A. Z. & Davis, R. A. 1997 Buoyancy-driven coalescence of slightly deformable drops. *J. Fluid Mech.* **346**, 117–148.

Stone, H. A. 1994 Dynamics of drop deformation and breakup of viscous fluids. *Ann. Rev. Fluid Mech.* **26**, 65–102.

Stone, H. A. & Brenner, M. P. 1996 Note on the capillary thread instability for fluids of equal viscosities. *J. Fluid Mech.* **318**, 373–374.

Yiantsos, S. G. & Davis, R. H. 1991 Close approach and deformation of two viscous drops due to gravity and van der Waals forces. *J. Colloid Interface Sci.* **144**, 412–433.